

Efficient Quantum Circuit Design with a Standard Cell Approach

Evan E. Dobbs,¹ Joseph S. Friedman,¹ and Alexandru Paler^{2,1}

¹*University of Texas at Dallas, Richardson, TX 75080, USA*

²*Aalto University, Espoo 02150, Finland*

We design quantum circuits by using a standard cell approach. Standard cells are a representation before deciding to compile either NISQ or surface code lattice surgery circuits. This approach can speed-up the layout of circuits with a regular structure. Our approach to co-designing quantum circuits can be used to estimate the resources necessary for the computation without effectively using complex compilation methods. Furthermore, we form standard cells to support Toffoli gate decompositions and starting from a 3D design of a multiplication circuit, we present evidence that, compared to the existing quantum circuit compilers, our method achieves shallower 3D circuits (by at least 2.5x) and with less SWAPs.

I. Introduction

The qubit layout of a quantum computer is, in general, very regular and similar to a tiling. For example, NISQ devices are tilings of various polygons such as squares (Google Sycamore), octagons and squares (Rigetti Aspen), or rectangles (IBM Hummingbird). Most of the devices are 2D, but there also exist 3D proposals such as for neutral atoms [1]. Tilings appear also in error-corrected quantum circuit layouts, where a simple example is the 2D tiling of rectangular patches used in surface code lattice surgery [2, 3]. For this reason, in the following, we design circuits by tiling standard cells.

A. Motivation

This work is motivated by the need to quickly compile quantum circuits as resource efficient as possible. Compilation speed is advantageous when estimating the resources necessary to run a circuit. It is also useful to evaluate how a qubit layout influences the compiled circuit. For example, some circuits may be suitable for 3D qubit layouts, while others only for 2D layouts. Such systematic design explorations have not yet been performed in the quantum circuit design literature.

Quantum circuits are often formed from repeating patterns of sub-circuits. This is the case for Toffoli+H circuits which consist entirely of the three-qubit Toffoli gate and the single-qubit Hadamard gate. The Toffoli gate is implemented by a Clifford+T sub-circuit. The Toffoli gate can be mapped to a cubic structure and there is a connection between the gate and colour codes [4]. Larger codes can be obtained by tiling unit cells representing smaller codes [4]. Analogous to those works, herein we tile Toffoli gates (cf. Fig. 1). The goal is to cover as much as possible a device’s qubit lattice.

After compiling a Toffoli+H circuit to Clifford+T, its depth can be improved by parallelising T gates [5–7] (sometimes using ancillae). For most practical quantum circuits, even by adding ancillae, there does not seem to exist an obvious systematic way to increase gate parallelism. Circuit depth and gate parallelism are not fixed

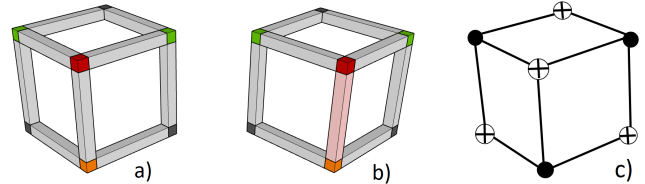


FIG. 1. The cube as a standard cell for a Toffoli gate implemented in 3D space in Clifford+T: a) Green vertices are the control qubits of the Toffoli gate, and the orange vertex is the target. In the Toffoli decomposition the orange and green qubits are CNOT controls and the grey qubits are CNOT targets; b) Pink edges represent SWAPs (will be used in Section III for visualising circuit extraction); c) Reading a NISQ circuit from a cell is performed by replacing each vertex with a qubit, and choosing a gate that corresponds to the sticks. Assuming that T and H gates are also executed on the vertices, the circuit from (c) will correspond to Fig. 8. Note that the cube is not a full cube and only has seven vertices.

costs, but functions of the device capabilities.

Compilation is a complex and time intensive task and most of the solutions are based on inserting SWAP or similar gates (e.g. [8, 9]). The resulting circuit can be up to one order of magnitude deeper than the original. This problem appears also for error-corrected circuits, such as when using lattice surgery surface code patches [3].

To reach near-optimal circuit design solutions within a reasonable time, we adapt the well-established standard cell approach from very-large-scale integration (VLSI) of conventional complementary metal-oxide-semiconductor (CMOS) transistors [10]. In the conventional VLSI standard cell approach, a library of optimized circuit blocks are interconnected as tiles within a large computing system. This is in contrast to full-custom design, in which each transistor is individually designed in a fully custom manner; while full-custom design permits full optimization to meet design specifications, it is intractable when billions or trillions of transistors are considered. The standard cell approach sacrifices optimality in order to drastically reduce the design time and complexity of design algorithms/heuristics, making it possible to design VLSI circuits with near-optimal performance and efficiency.

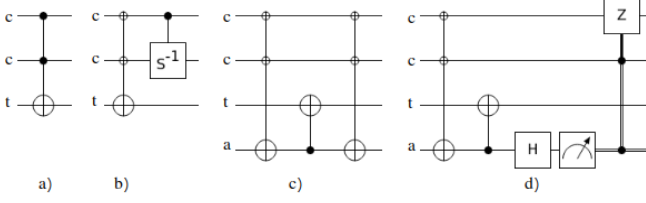


FIG. 2. The Toffoli gate from a) can be implemented using: b) an AND gate and a controlled-S gate, c) an ancilla initialised in $|0\rangle$, two AND gates and a CNOT, d) an AND, an ancilla, and a CNOT; here the uncomputation is measurement-based. The wire labels denote [c]ontrol, [t]arget, and [a]ncilla.

B. Related Work

As the design and optimization of quantum circuits becomes intractable when scaled to large circuits, we propose that standard cell design approaches are suitable for the design of near-optimal quantum computing systems within reasonable design time constraints.

FPGA-like approaches to quantum circuit compilation have been proposed, for example, in [11–14]. Those approaches use also cells, but those are configurable, programmable elements laid out in such a way that arbitrary computations can be implemented. In contrast, our cells are *non-configurable, pre-programmed* elements. We do not have a cell for routing, like in [15], because we are extracting SWAP schedules after the circuit has been tiled.

Tiles for error-corrected circuits have been presented, for example, in [15, 16]. Our tiles operate at a higher level and mediate between logical circuit and physical implementation: we extract both error-corrected as well as NISQ circuits from the same tiled structure.

Our cells are compatible with the connectivity of the underlying device. Our design method is the opposite of the one presented in [17] in which gates are scheduled neglecting connectivity considerations, while routing operations are added at a later step.

Standard cells have also been proposed for other emerging computing platforms, such as quantum-dot cellular automata [18, 19] where tiles are placed and routes are computed between the tiles.

In the process of preparing the manuscript, we became aware of parallel efforts of using tiles for co-designing quantum circuits. The differences between our approach and those methods is that the latter use tiles which: a) are designed for each type of computational primitive (e.g. CNOT, Hadamard, routing), b) are used for automatic NISQ-level error-analysis; c) cannot be used for extracting surface-code computations.

C. Contributions

We introduce standard cells, in the following also called *tiles*, and we arrange the cells to represent the structure of a given circuit (e.g. adder, multiplier). We join tiles

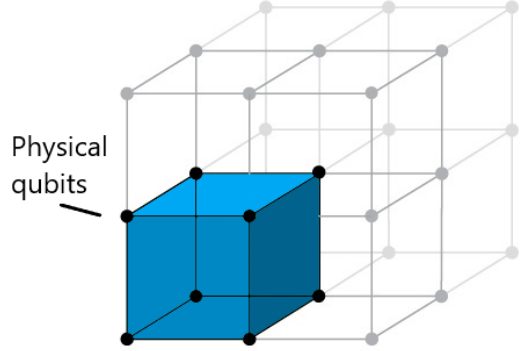


FIG. 3. An example of co-design: quantum circuits are built from cells which are designed specifically for the underlying hardware architecture. The hardware is a 3D qubit lattice, and the standard cell, such as the one from Figure 1, will fit in the blue region. For clarity, we will use cubic vertices to represent the computational qubits of the circuit constructed on the physical qubit lattice.

into layouts that represent the structure of the circuit to be compiled. The complete layout will include *queue-like qubit storage* for qubits not involved in the computation. The complete quantum circuit is obtained from the layout after computing the qubit movement from the storage across the tiles. We *extract schedules* (ie. quantum circuits whose gates are in well defined order) from the tiled structures and can be easily translated into either NISQ or error-corrected lattice surgery circuits[2].

Our tiles are useful, for example, for Toffoli+H circuits. Toffoli gates cannot, in general, be executed natively, and are decomposed into sequences of Clifford+T gates. The latter are compatible with the NISQ device or the error-correcting code. The Hadamard gate is comparatively straightforward to execute on almost any computer. A Toffoli gate can be obtained from an AND gate and a controlled-S gate. When using measurement-based uncomputation [6] and an ancilla, the Toffoli gate can be implemented with a single AND gate. These circuits are illustrated in Fig. 2.

We consider quantum computers having the qubits arranged into lattices. Our work focuses on 3D lattices. For completeness we start by sketching a 2D approach where the unit cell is a square that is tiled along both directions. The unit cell in the 3D case is a cube tiled in three dimensions.

II. Methods

We propose a circuit design method that starts from the observation that physical hardware qubit lattices as well as the quantum circuit that will be compiled both have a very regular structure (e.g. Fig. 3).

A *standard cell* is a pattern that represents the 2D/3D abstraction of the qubits and the gates that form a sub-circuit (e.g. the Clifford+T decomposition of the Toffoli gate). *Tiling* is the procedure by which circuits are de-

signed in a manner that is automatically compatible with the underlying qubit lattices. *Scheduling* is the method that outputs the order in which the Clifford+T gates of the original circuit will be executed. As a result, a *schedule* is a quantum circuit that includes gate parallelism information.

The tiled structure includes *lines* called *qubit storage*. The storage works like a queue: qubits are pushed and popped from the storage using SWAP operations. We analysed the functionality of such queues for the restricted case of a four qubit multiplication circuit in [20].

A tiled structure supports a computation whose execution is a repetition of two steps: 1) apply single- and two-qubit gates (except qubit movement operations such as SWAPs) according to the connectivity; 2) move qubits on the layout in order to support the next application of gates. This approach is explained in this section and will be exemplified in Section III and Fig. 10.

Our tiles are designed (pre-programmed) for computations where no SWAP gates are necessary. For example, no SWAPs are required in order to perform the Toffoli gate on the tile from Fig. 1. Our tiling method simplifies the analysis of efficient SWAP insertion and scheduling.

In this work, we tile Toffoli+H circuits by considering tiles for the Toffoli gates. The challenges are to find Toffoli tiles which can be efficiently tiled to qubit lattices, and to generate circuits of shallow depth.

A. Tiling: Mapping tiles to a qubit lattice

A standard cell is a qubit layout where the allowed two-qubit interactions are represented by sticks. This means that, for the example of Fig. 1, the grey sticks of a tile can support any two-qubit gate. For the purpose of this work, we consider that each tile corresponds to a single type of Toffoli gate decomposition.

We employ a graph representation for the tiled Toffoli gates, and use cells which are compatible with the square 2D and cubic 3D arrangement of qubits. The cell represents where qubits are placed and which qubit interactions will be performed. However, a *standard cell does not capture the order of the interactions*. This means that the circuit and its depth cannot be read immediately from the tiling.

Fig. 1 shows a 3D tile. Coloured vertices are qubits: grey and red are ancillae, green for Toffoli control qubits, and orange for Toffoli target qubits. We do not explicitly mark the cubes where Hadamard gates are applied, because these can be applied on any type of vertex colour. Because a qubit can change its functionality between being control and target, we will draw the same cube twice – one next to the other.

The third dimension in 3D does not represent time, but simply the three-dimensional arrangement of the qubits. With a time axis, the 3D qubit lattice would generate a 4D space-time volume. A 3D tile can be used for extracting 3D NISQ or 3D surface code circuits [21]. In

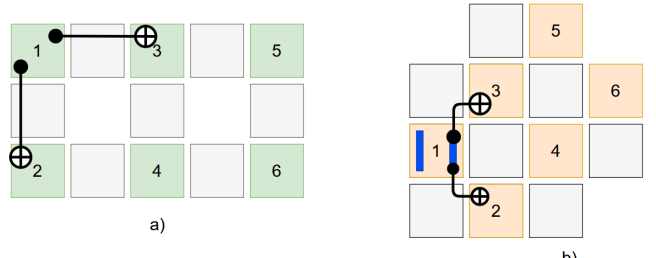


FIG. 4. a) Top perspective of two tiles (the green patches correspond to vertices like in Fig. 1) sharing an edge (grey patch between green patches 3 and 4). b) Orange patches correspond to the green patches from before, but this time the layout is such that the classic [2] lattice surgery CNOT can be implemented. The layout of orange patches is obtained after *rotating* the diagram from (a). The grey ancilla patch is used interchangeably between the lattice surgery tiles (cf. the pattern for CNOT and how the boundaries are arranged herein).

Section III we present a quantum multiplication circuit which was designed by tiling 3D tiles.

B. Scheduling: Reading parallelized circuits

The same unit cell can be used to support more than a single sub-circuit. Moreover, a tile, e.g. Fig. 1, can be used to read NISQ circuits as well as surface code protected quantum circuits. For NISQ, the grey sticks connecting the vertices are two qubit gates (e.g. CNOT, CZ). The (almost) circuit diagram from Fig. 1 is very similar to a ZX diagram [22], but this is only because we have chosen to translate the sticks with CNOTs.

For reading error-corrected circuits, we consider the surface code implemented by lattice surgery (Fig. 4 and Appendix). There are two options when translating tilings to surface code operations. The first option incorporates 2D tilings, e.g. Section II C, where the sticks represent merge and split operations. The second option incorporates 3D tilings, which can be interpreted as layered 2D tilings: within a layer the sticks are lattice surgery operations, and between layers the sticks are surface code transversal operations [2]. In 3D tilings, e.g. Fig. 1(a), the sticks connecting the upper and lower layers (e.g. red to orange stick) are transversal CNOTs, for example.

C. Standard Cells for 2D and 3D Architectures

The three qubits of the Toffoli gate make it almost a perfect candidate for nearest neighbour 2D or 3D interactions. The AND gate from [6] is already compatible with 2D without requiring any SWAP gates. The Toffoli gate from [23] as well as the one from [24] require only a few SWAPs to be implemented in 2D. In the following, we use a low depth, natively 2D compatible Toffoli gate

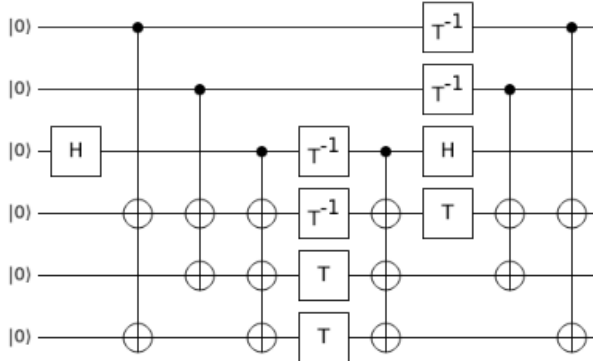


FIG. 5. The T-depth two circuit that uses three ancillae is obtained by combining the Clifford+T circuits for an AND and controlled-S gate. The two CNOTs of Fig. 16 in the Appendix do not need to be applied because the corresponding ancilla wire has already computed the necessary bit parity.

circuit (the derivation is in the Appendix). We use ancillae as in [6], a T-depth of 2, and (depending on how the depth of the CNOTs is counted) a total depth ranging from 6 to 9.

The 2D tile we propose in Fig. 6 is based on the circuit from Fig. 5. It is obtained by placing the ancilla qubits (gray vertices) between the data qubits (green and orange vertices), and by observing that the CNOTs can be implemented in a nearest-neighbour manner. For example, the ancilla targeted by three CNOTs is placed at the crossing of the sticks from the green and orange vertices.

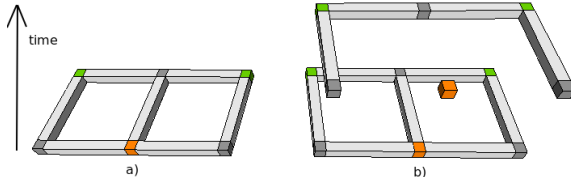


FIG. 6. Tile for Toffoli T-depth two (control qubits are green, target is orange): a) the 2D layout to implement Fig. 15, b) the layout for Fig. 16 is on top of the AND. Because (a) and (b) have the same layout, the tile to implement the 2D T-depth two Toffoli is the one from (a).

The 2D cell can also be used for implementing computations in 3D (see Fig. 7). The 2D case shows that, if enough qubits are available: a) Toffoli tiles can be easily arranged on a Sycamore-like device; and b) it can reduce the routing overhead necessary for implementing lattice surgery computations (cf. [3, 25]). However, the circuit in Fig. 5 includes 14 CNOTs compared to the six that represent the optimum for the Toffoli decomposition [26]. If one accounts for the SWAPs necessary for nearest neighbour interaction in the standard Toffoli decomposition [23], the CNOT cost reaches 9.

Nevertheless, the advantage of the T-depth two decomposition and associated tile is its shallower total depth (i.e. reducing depth by increasing the number of CNOTs).

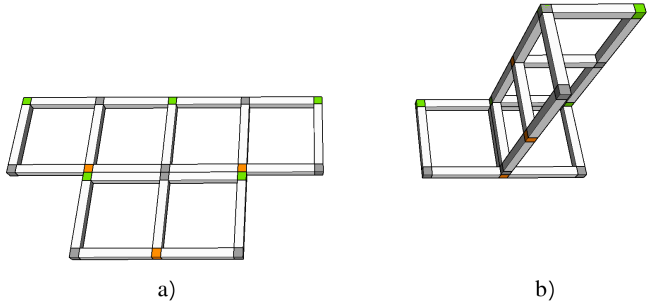


FIG. 7. Example of using the 2D tile in: a) square two-dimensional lattice; b) cubic three-dimensional lattice. In this figure, as well as in others, whenever two qubits appear adjacent and have different colours it implies that they support different functionalities at different stages of the computation (e.g. the same qubit can be the target of one Toffoli gate and the control of another).

We also design a 3D specific cell (cf. Fig. 1), which is compatible with the T-depth one Toffoli gate decomposition illustrated in Fig. 8. This decomposition has the advantage that, in the best case, it has an overall depth of three (if the computing architecture supports CNOT parallelism). There is a connection between the T-depth one Toffoli gate decomposition and colour codes [27]. In this work, the tiles represent Toffoli gates, and the fact that there is a connection between tiles and colour codes [4] indicates that quantum circuits can be built similarly to how larger codes are constructed by repeating patterns of qubit layouts.

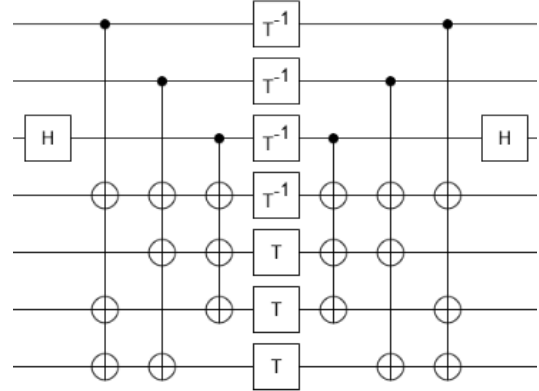


FIG. 8. The T-depth 1 CCZ gate decomposition [7].

III. Results

Practical quantum circuits have a regular structure. For example, the regularity can be noticed in large scale computations where quantum arithmetic functionality is often used as a sub-circuit. For example, the ripple-carry adder has a V-shape of Toffoli gates. Quantum multiplication circuits are built on top of quantum addition.

In this work, we manually construct the multiplier circuit (see Appendix for its circuit diagram) from [28] by tiling cubic tiles as in Fig. 1. We compare the results from this manual tiling to the automatically mapped and routed multiplication circuits from [28]. In future work, the superiority of our proposed tiling approach will translate to drastic improvements in the automation of large-scale quantum circuit design.

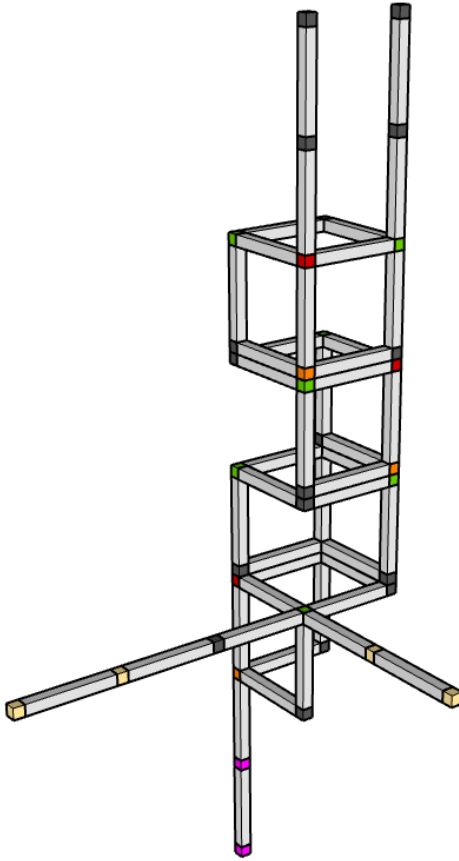


FIG. 9. The structure of the multiplier resulting from tiling Toffoli cubes and adding requisite ancillae to implement the controlled addition sub-circuits in a three-dimensional lattice. The lines of qubits extending out of the figure are queues meant to hold qubits to be used in later iterations within the multiplier. Specifically, the upper-left queue holds ancillae which will swap with qubits from the B register, the upper right queue holds qubits from the product register, the magenta queue on the bottom holds ancillae which will eventually swap with members of the product register, and the yellow queues going out hold the B operand as well as the designated ancillary qubit Z (the sole grey qubit among the yellow qubits in the queue). These queues are often depicted in abbreviated forms in other figures for the sake of readability, and in fact their form is arbitrary as they will always be chains of qubits.

A. Compiling using Standard Cells

The tiling from Fig. 9 is for a four qubit multiplier from [28]. The multiplication circuit computes the product in a register that is disjoint from the multiplicand registers A and B . The multiplier consists of: 1) a Toffoli step and 2) $n-1$ Ctrl-Add (controlled addition) steps. Some of the control signals necessary for the Ctrl-Add steps have to be available next to the Toffoli gate that is executed at a given moment. Our tiling was obtained after including some structural circuit optimisations.

The *yellow storage* in Fig. 10 holds qubits from the B register to be used in later iterations (i.e. those which are used as the control qubit in each iteration), the magenta storage holds elements of the product register to be used in later iterations grey (top), and the grey storages hold elements of the product and B registers which will not be used again in the computation, with the left and right storages holding B register and P product register qubits respectively.

B. Extracting Parallelized Circuits

We illustrate the gate scheduling of the tiled multiplication circuit. We analyse the cost in terms of SWAP gates necessary to execute the circuit. We have chosen to not introduce additional qubits and to perform SWAPs only across the multiplication tiling. For example, the number of SWAPs could be improved by adding a *vertical tower* parallel to the existing structure.

Fig. 10 (and Figs. 19, 20 and 21 from the Appendix) demonstrate visually each moment of SWAPs during the circuit, where a red bar between two qubits represents a SWAP gate being applied between them. So Fig. 10 demonstrates each step of SWAPs necessary to implement the Toffoli step of the sample 4-qubit multiplier. Note that these figures only represent SWAP moments, so the application of Toffoli gates is not shown (though they are present in the schedules below).

In the following, we present one the algorithms used for extracting the schedules. In the Appendix we present the algorithms for the other steps. In the listings, “upper” and “lower” refer to the top and bottom of the Toffoli-cube being worked in respectively; e.g. “lower W” refers to the ancillary qubit in the West corner of the bottom 4 corners of the current Toffoli-cube. “N” is for North. Multiple gates listed on a line are in the same moment (a *moment* represents all the gates that can be executed in parallel).

```

1 Repeat for each a and b
2   Toffoli (ctrl, a0, b0)
3   SWAP (ctrl, W), SWAP(a0, N)
4   SWAP (ctrl, b0), SWAP (a0, N)
5   SWAP(b0, ancilla directly above)
6 Until just before the nth cube.
7
8 Toffoli(ctrl, an-1, bn-1)
9 SWAP(an-1, S), SWAP(bn-1, bn)

```

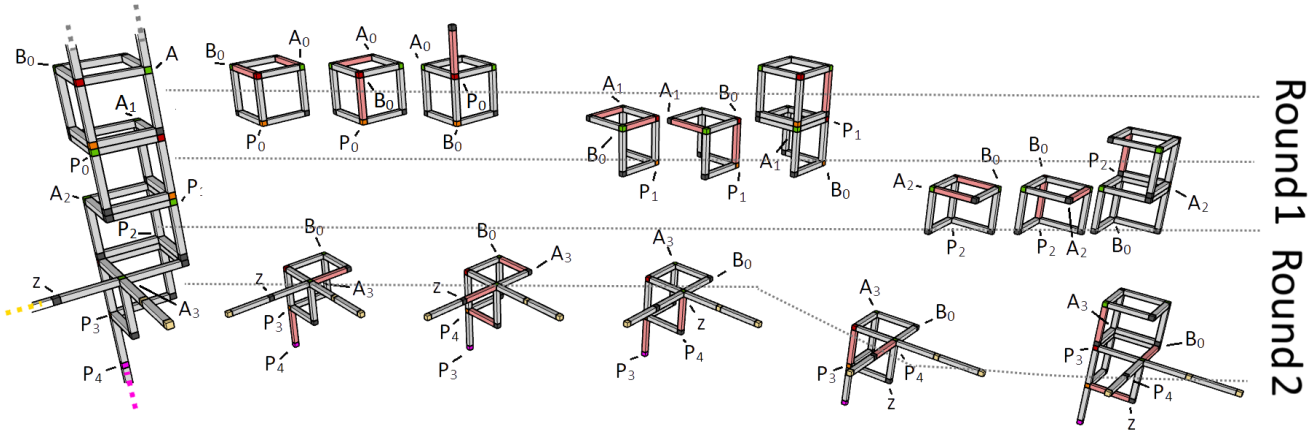


FIG. 10. SWAP schedule for the Toffoli step of the 3D multiplier circuit. Red bars indicates the application of a SWAP gate between two qubits. The initial mapping of the qubit registers to be multiplied (A and B) is indicated with labels of the form A_i, B_i . The product register is P , and Z is an ancilla. In this step of the multiplication, a Toffoli gate is applied to each qubit P_i of the product register, with the corresponding A_i and B_0 qubit acting as controls. With respect to the scheduling procedure from Listing 1, there are two rounds: Round 1 represents three repetitions of Line 1, one per tile/cube. Round 2 represents Lines 9-14. On each row, time flows from left to right. The coloured dotted lines represent the extension of the qubit queues. The gray dotted lines indicate the position of the tile in the left hand side figure where the SWAP gates are performed. The mapping of the qubits illustrated on the left hand side figure is changing during the execution of the schedule (ie. qubits are swapped). For example, in Step 2, after being swapped, B_0 is close to the Z ancilla.

```

10 SWAP(W, z), SWAP(bn, lower W), SWAP(an-1, ctrl)
11 SWAP(bn, z), SWAP(bn-1, lower N)
12 SWAP(bn, empty space in queue), SWAP(bn-1, upper N)
13 SWAP(bn-1, N above current position), SWAP(z, lower N), SWAP(ctrl, W)
14 SWAP(ctrl, next ancilla (B qubit) in queue))

```

Listing 1. The Toffoli step schedule.

Throughout the schedule, gates are typically applied to either some combination of $ctrl$, z , a_j , and p_j , where j is the largest subscript in the current iteration, or to each of a_i and b_i for every cube i , where a and b refer to the registers of the first and second operands of the current controlled addition step respectively (in the case of the Toffoli step, these refer to the operands of the first controlled-addition step). In the former case, qubits must be swapped around the very small space in the final cube, while in the latter case $ctrl$ is swapped up the tower to be used in each cube.

IV. Discussion

Tiling is a way of compiling circuits for a device that has a regular layout of qubits. This is a co-design approach towards the compilation of circuits. We illustrated tiling using 2D and 3D tiles which were specifically designed for square and cubic qubit lattices. As an example, we obtained a multiplier by tiling cubes representing Toffoli gates. We then scheduled the execution of the circuit, effectively extracting the parallelized version of the multiplication circuit. In the following, we discuss the efficiency of tiling from the perspective of gate counts and depths as well as from the hardware usage ratio.

A. Improved Gate Counts and Depths

One of the disadvantages of the current generation of quantum circuit mapping and compilation methods is their inefficiency with respect to execution times [29], as well as their inability to compile optimal circuits with respect to SWAP gate counts and depths.

For our tiled multiplication circuit example, the upper bound on the SWAP gate metrics (the SWAP gate count $SwapC$, and the SWAP gate depth $SwapD$) is determined by the two types of steps: Toffoli and Ctrl-Add. For the Toffoli step which occurs once in the multiplier:

$$SwapC_t = 5(n-1) + 12$$

$$SwapD_t = 2(n-1) + 5$$

$SwapD_t$ can be lowered to $2(n-1)$ considering that the last step can be always parallelized with the next Toffoli.

For Ctrl-Add steps we have the following:

$$SwapC_{ca} = 6(n-1) + 16$$

$$SwapD_{ca} = 4(n-1) + 10$$

Again, $SwapC_{ca}$ may be lowered when considering the real CNOT cost of the SWAPs. The Ctrl-Add circuits swap adder qubits with ancillae in $|0\rangle$. For these operations it is sufficient to have SWAPs formed of two CNOT gates. $SwapD_{ca}$ may also be improved when considering Toffoli gate parallelism.

There are also SWAPs taking place between the Ctrl-Add steps. These SWAPs occur for $n-2$ times:

$$SwapC_b = 4(n-1) + 9$$

$$SwapD_b = 5$$



FIG. 11. Automatically routed circuits vs. tiled circuits – SWAP depth and count for different multiplication circuit sizes. The left chart compares SWAP counts and the right chart SWAP Depth. The horizontal axis in both charts represents the size of the multiplication (e.g. a 4-bit multiplication), and the vertical axis is the number of SWAP gates and the number of SWAP moments required respectively. The green bars are our tiled multiplier, whereas the red bars are the automatic Google Cirq routing. We conclude that tiling, for these kind of circuits, is more resource efficient.

As a result, the total number of SWAPs, not including the ones in qubit storage (their depth is 0 because they are in parallel with other SWAPs in the circuit, and their count is order of $\mathcal{O}(n^2)$):

$$\begin{aligned} SwapC &= SwapC_t + (n-1)SwapC_{ca} + (n-2)SwapC_b \\ &= 10n^2 + 6n - 13 \end{aligned}$$

$$\begin{aligned} SwapD &= SwapD_t + (n-1)SwapD_{ca} + (n-2)SwapD_b \\ &= 4n^2 + 5n - 13 \end{aligned}$$

B. Efficiency

Standard cells are advantageous, but these still do not completely solve the need for almost arbitrary all-to-all connectivity, and SWAP gates are still required to implement arbitrary computations. Nevertheless, one of the advantages of tiling is that it simplifies the calculation of the SWAP networks necessary during the computation.

When compared with automatic routing methods, such as the ones available in Google Cirq, our tiled version of the multiplier improves significantly on both SWAP depth and count, as demonstrated by Fig. 11. The SWAP depth and count numbers for Cirq were obtained by providing the router with a 3D device of the same general dimensions as our tiled circuit and allowing it to route greedily. In many cases the router was actually provided with more qubits than the tiled circuit uses. For additional details and source code see the repository at [30].

We define the *usage ratio* as the tile qubits to the total number of computer qubits necessary to hold the tiling. In the case of a single 3D tile we use seven qubits, and if the hardware would look like a cube (has eight vertices), the *usage ratio* would be 7/8. If one considers that only three are computational qubits and four are ancilla, then the effectiveness ratio is 3/8. Another perspective is that four qubits are needed in order to achieve high parallelism in a 3D layout.

A more detailed analysis of the usage and effectiveness ratios for the multiplier shows that, after some optimization on the positioning and structure of qubit storages, the multiplier can achieve a usage ratio of 33/48 for the 4-qubit case. Generalized, the multiplier requires $2*3*(N+1+[N/4]+[N/2])$ qubits, and uses some number less than this. Note that the portion of the above equation in parentheses represents the height of the multiplier structure, whereas the width and length remain constant as 2 and 3. This information is relevant as it provides for a highly regular final structure for a quantum arithmetic circuit, which is likely to be repeated many times throughout a given computation.

V. Conclusion

Standard cells and tiling form a powerful step for compiling logical quantum circuits on physical devices, both NISQ and error-corrected. First, tiling quantum circuits can inform the co-design of computing architectures, where the qubit layout, for example, is developed in parallel to the circuits to execute. Such 2D and 3D architectural co-design can be implemented with neutral atoms [1], for example, and future work will focus on NISQ-aware tilings for such architectures. Second, the relation between our Toffoli tiles and quantum error-correcting codes and quantum error mitigation techniques, e.g. [31], make tiling an interesting candidate for the co-design of circuits in the presence of fault-tolerance preserving methods.

Tiling standard cells allows for a faster and improved understanding of the layout of the compiled circuit without the processing time involved in compilation and routing. Tiling is especially useful for highly regular, frequently repeated sub-circuits such as those in quantum arithmetic. It is a valuable tool in estimating the resources required for compiling a given quantum circuit to hardware, and especially in creating structures which have highly parallel SWAP schedules.

We presented an application of tiling with respect to multiplication circuits. Our method relied on a tile of a T-depth two Toffoli decomposition in both 2D and 3D. We placed the tile repeatedly in a regular structure to effectively represent regular quantum circuits. We demonstrate the effectiveness of our method by using it to design a quantum multiplier, showing its usefulness for scheduling SWAP gates by significantly improving on both the SWAP depth and count of the circuit over existing automatic routing methods.

Future work will focus on tiling as a means to reduce the number of qubits which are inaccessible in large,

error-corrected computations by virtue of the regular structure of the models it creates. In other words, tiling could be used to improve the usage ratio of the chip as a whole, as discussed in section IV.

Acknowledgments

We thank George Watkins for feedback on a preliminary version of this manuscript.

[1] L. Henriet, L. Beguin, A. Signoles, T. Lahaye, A. Browaeys, G.-O. Reymond, and C. Jurczak, Quantum computing with neutral atoms, arXiv preprint arXiv:2006.12326 (2020).

[2] C. Horsman, A. G. Fowler, S. Devitt, and R. Van Meter, Surface code quantum computing by lattice surgery, *New Journal of Physics* **14**, 123011 (2012).

[3] D. Litinski, A game of surface codes: Large-scale quantum computing with lattice surgery, *Quantum* **3**, 128 (2019).

[4] D. A. Lidar and T. A. Brun, *Quantum error correction* (Cambridge university press, 2013).

[5] M. Amy and M. Mosca, T-count optimization and reed-muller codes, *IEEE Transactions on Information Theory* **65**, 4771 (2019).

[6] C. Jones, Low-overhead constructions for the fault-tolerant toffoli gate, *Physical Review A* **87**, 022328 (2013).

[7] P. Selinger, Quantum circuits of t-depth one, *Physical Review A* **87**, 042302 (2013).

[8] G. Li, Y. Ding, and Y. Xie, Tackling the qubit mapping problem for nisq-era quantum devices, in *Proceedings of the Twenty-Fourth International Conference on Architectural Support for Programming Languages and Operating Systems* (2019) pp. 1001–1014.

[9] C. Zhang, A. B. Hayes, L. Qiu, Y. Jin, Y. Chen, and E. Z. Zhang, Time-optimal qubit mapping, in *Proceedings of the 26th ACM International Conference on Architectural Support for Programming Languages and Operating Systems* (2021) pp. 360–374.

[10] A. B. Kahng, J. Lienig, I. L. Markov, and J. Hu, *VLSI physical design: from graph partitioning to timing closure* (Springer Science & Business Media, 2011).

[11] T. Serdar and C. Sechen, Automatic datapath tile placement and routing, in *Proceedings Design, Automation and Test in Europe. Conference and Exhibition 2001* (IEEE, 2001) pp. 552–559.

[12] M. Suchara, J. Kubiatowicz, A. Faruque, F. T. Chong, C.-Y. Lai, and G. Paz, Qure: The quantum resource estimator toolbox, in *2013 IEEE 31st International Conference on Computer Design (ICCD)* (IEEE, 2013) pp. 419–426.

[13] L. Lao, B. van Wee, I. Ashraf, J. van Someren, N. Khammassi, K. Bertels, and C. G. Almudever, Mapping of lattice surgery-based quantum circuits on surface code architectures, *Quantum Science and Technology* **4**, 015005 (2018).

[14] M. Ahsan and J. Kim, Optimization of quantum computer architecture using a resource-performance simulator, in *2015 Design, Automation & Test in Europe Conference & Exhibition (DATE)* (IEEE, 2015) pp. 1108–1113.

[15] M. Ahsan, R. V. Meter, and J. Kim, Designing a million-qubit quantum computer using a resource performance simulator, *ACM Journal on Emerging Technologies in Computing Systems (JETC)* **12**, 1 (2015).

[16] A. Shafaei, M. J. Dousti, and M. Pedram, Computer-aided design for next-generation quantum computing systems, *International Journal of Theoretical Physics, Group Theory, and Nonlinear Optics* **19**, 69 (2015).

[17] G. G. Guerreschi and J. Park, Two-step approach to scheduling quantum circuits, *Quantum Science and Technology* **3**, 045003 (2018).

[18] D. A. Reis, C. A. T. Campos, T. R. B. Soares, O. P. V. Neto, and F. S. Torres, A methodology for standard cell design for qca, in *2016 IEEE International Symposium on Circuits and Systems (ISCAS)* (IEEE, 2016) pp. 2114–2117.

[19] M. Walter, R. Wille, D. Große, F. S. Torres, and R. Drechsler, Placement and routing for tile-based field-coupled nanocomputing circuits is np-complete (research note), *ACM Journal on Emerging Technologies in Computing Systems (JETC)* **15**, 1 (2019).

[20] E. E. Dobbs, R. Basmadjian, A. Paler, and J. S. Friedman, Fast swapping in a quantum multiplier modelled as a queuing network, in *International Conference on Reversible Computation* (Springer, 2021) pp. 256–265.

[21] M. Vasmer and D. E. Browne, Three-dimensional surface codes: Transversal gates and fault-tolerant architectures, *Physical Review A* **100**, 012312 (2019).

[22] J. van de Wetering, Zx-calculus for the working quantum computer scientist, arXiv preprint arXiv:2012.13966 (2020).

[23] M. A. Nielsen and I. L. Chuang, *Quantum Computation and Quantum Information* (Cambridge University Press, 2010).

[24] C. Gidney, Halving the cost of quantum addition, *Quantum* **2**, 74 (2018).

[25] A. Paler and A. G. Fowler, Opensurgery for topological assemblies, in *2020 IEEE Globecom Workshops (GC Wkshps)* (IEEE, 2020) pp. 1–4.

[26] V. V. Shende and I. L. Markov, On the cnot-cost of tof-

foli gates, *Quantum Information & Computation* **9**, 461 (2009).

[27] E. T. Campbell, *The smallest interesting colour code*, available at <https://earltcampbell.com/2016/09/26/the-smallest-interesting-colour-code/>.

[28] E. Muñoz-Coreas and H. Thapliyal, Quantum circuit design of a t-count optimized integer multiplier, *IEEE Transactions on Computers* **68**, 729 (2018).

[29] A. Paler and R. Basmadjian, Energy cost of quantum circuit optimisation: Predicting that optimising shor's algorithm circuit uses 1 gwh, *ACM Transactions on Quantum Computing* **3**, 1 (2022).

[30] E. E. Dobbs and A. Paler, *Source code*, available at <https://github.com/alexandrupaler/tilingquantumcircuits>.

[31] R. Chao and B. W. Reichardt, Quantum error correction with only two extra qubits, *Physical review letters* **121**, 050502 (2018).

[32] M. Y. Siraichi, V. F. d. Santos, S. Collange, and F. M. Q. Pereira, Qubit allocation, in *Proceedings of the 2018 International Symposium on Code Generation and Optimization*, CGO 2018 (Association for Computing Machinery, New York, NY, USA, 2018) p. 113–125.

[33] B. Dury and O. Di Matteo, A qubo formulation for qubit allocation, *arXiv preprint arXiv:2009.00140* (2020).

[34] A. Barenco, C. H. Bennett, R. Cleve, D. P. DiVincenzo, N. Margolus, P. Shor, T. Sleator, J. A. Smolin, and H. Weinfurter, Elementary gates for quantum computation, *Physical review A* **52**, 3457 (1995).

[35] G. Song and A. Klappenecker, The simplified Toffoli gate implementation by Margolus is optimal, *arXiv preprint quant-ph/0312225* (2003).

[36] A. Paler, O. Oumarou, and R. Basmadjian, On the realistic worst case analysis of quantum arithmetic circuits, *arXiv preprint arXiv:2101.04764* (2021).

Appendix

Tiling is very similar to the qubit allocation problem (e.g. [32] for a recent approach). This time, multi-qubit tiles will be allocated instead of single qubits. Optimal tilings can be obtained using exact methods. For example, recently, qubit allocation has been formulated as a quadratic unconstrained optimisation problem [33], such that heuristic annealing approaches can be used to solve exact formulations of the allocation problem. Heuristics can also be used for tilings.

The circuit diagram for the ripple-carry adder and the multiplication circuit using it are illustrated in Fig. 12.

A. Lattice surgery layouts

The logical qubits are patches and arranged in an array like the one from Fig. 14(a). Each patch has two types of boundaries and two-qubit logical gates are implemented by merging and splitting patches along their boundaries [2, 3]. The type of the boundary that is manipulated determines the type of the operation. In Fig. 14(b) the

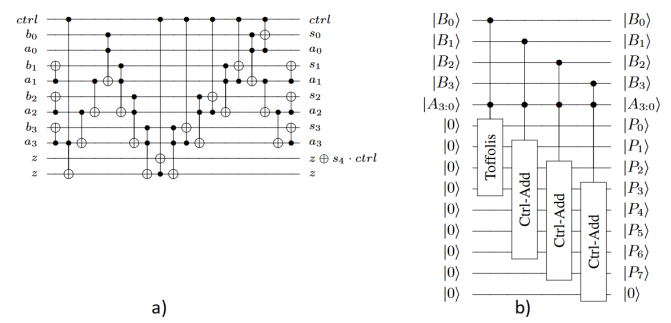


FIG. 12. Circuit from [28] which we used to construct tilings: a) the controlled-adder; b) the multiplier which is a sequence of controlled-adders.

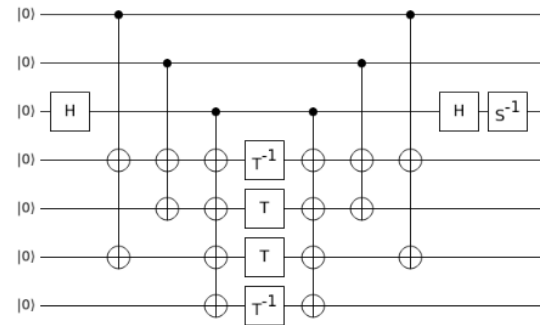


FIG. 13. Logical AND with four ancillae and T-depth 1. This circuit is obtained by removing four CNOTs and three T gates from the circuit from Fig. 8.

sequence of merge and splits is the standard way to implement a CNOT with lattice surgery, and the orange patch is an ancilla that mediates this operation.

The depth of the circuit depends on the hardware parallelism. In lattice surgery circuits, it is possible to parallelise CNOTs whenever the same qubit is used simultaneously as control or target. In 2D tilings, the maximum number of parallel CNOTs is two (two patch boundaries can be used simultaneously, cf. Fig. 4 where both non marked boundaries are used for two parallel CNOTs). In 3D tilings, at most four parallel CNOTs can be parallelised (two from the lattice surgery operations, and two more as transversal operations). The depth of the Toffoli gate decompositions can be as low as three when using 3D tiles, because the Clifford+T decomposition contains CNOTs that can be parallelised.

B. Construction of the T-depth two Toffoli

Fig. 15 is obtained similarly to the T-depth one Toffoli gate from [6] (Fig. 8) by placing the four T gates according to the AND gate phase polynomial. We follow the recipe from Fig. 2 and need a controlled-S gate next to the AND in order to build a Toffoli. Fig. 16 is the controlled-S gate of T-depth 1 using one ancilla. Finally,

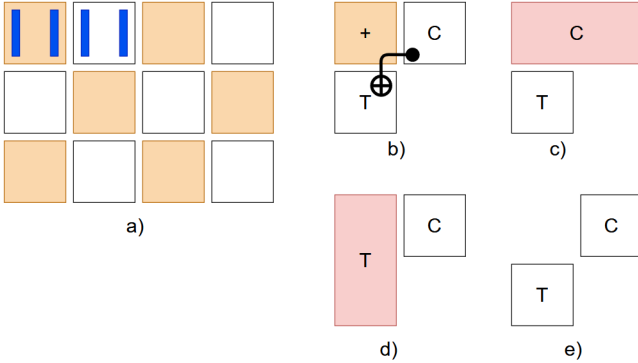


FIG. 14. Lattice surgery where qubits are patches: a) (orange) qubits with two types of boundaries, and (white) ancillae used to implement gates; b-d) the CNOT between two qubits is the sequence of the two merge and split operations (red) that involve the orange ancilla. The ancilla patch was initialised in $|+\rangle$ and measured after the red operations. For each patch, one boundary type is blue, the other is not coloured. For clarity, not all boundaries are drawn. The type of the operated boundaries is important. The superimposed CNOT in (b) is to show that the patch labelled "C" is the control, "T" is the target, and the orange patch mediates the CNOT.

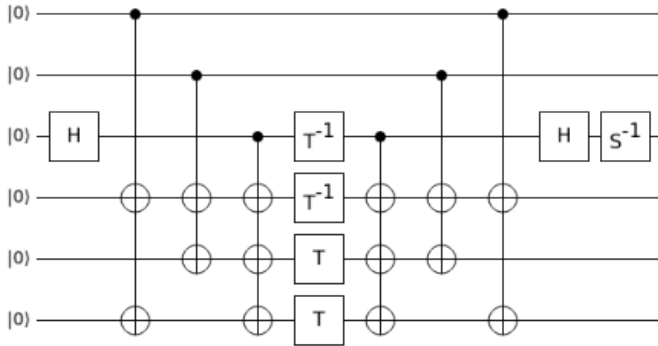


FIG. 15. Logical AND gate with three ancillae and T-depth 1. The total depth is seven, because CNOTs share the same control wire and can be parallelised. The H and S gate can be executed in parallel with their neighbouring CNOTs. This decomposition is obtained from Fig. 13 after removing two CNOTs and moving a T gate on the target (third) qubit.

we combine the Fig. 15 and 16 and obtain 5.

C. Tiles for measurement-based circuits

We presented scheduling tiles for Toffoli gates, but AND gates and measurement-based uncomputations can be as easily be extracted from the tilings. Fig. 17 is the implementation of the Toffoli by AND and measurements, and Fig. 18 shows how the 2D tile is obtained after scheduling the individual gates.

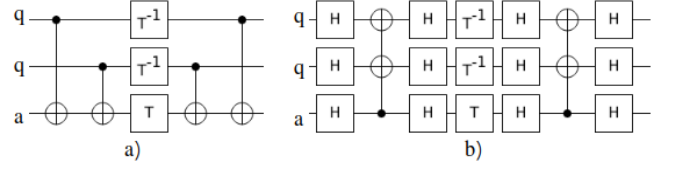


FIG. 16. Control-S gate with one ancilla and T-depth 1. a) Depth five Clifford+T decomposition. b) Equivalent but deeper circuit after inserting H gates. Wires are labelled [q]ubit and [a]ncilla.

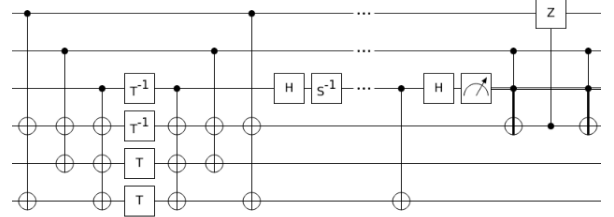


FIG. 17. The logical AND together with an ancilla can be used to implement a Toffoli gate with only 4 T gates. The ancilla is uncomputed in a measurement-based manner and a corrective control-Z gate is applied depending on the measurement result. Considering the 2D nearest-neighbour layout, the correction is mediated by an ancilla.

D. Toffoli, AND and Parallelism

The Toffoli gate is decomposed into CNOTs and seven T gates. The decomposition gates can be arranged in a vast number of circuit configurations as long as a set of conditions is fulfilled; these conditions are expressed as a phase polynomial [7]. One of the first Toffoli gate decompositions was presented in [34].

The *almost Toffoli* gate [35], which was initially described by Margolus, is implementing only up to a relative phase the Toffoli gate. This gate is also called the AND gate, and requires only four T gates in its decomposition – its phase polynomial has four terms. However, due to the relative phase, the AND gate cannot be easily used as a replacement for the Toffoli gate.

We did not focus on minimising T-count, but preferred minimum T-depth whenever possible. The T-count of a

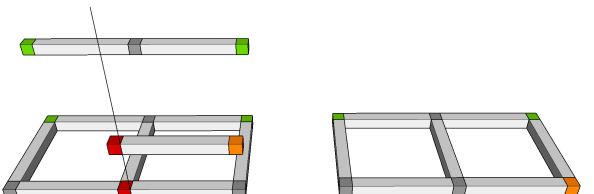


FIG. 18. The 2D layout to implement Fig. 17 (control qubits are green, target is orange). a) Three time steps stacked vertically: 1. the layout of the logical AND; 2. the CNOT from the AND qubit (red) qubit to the qubit that simulates the Toffoli target (orange); and 3. the measurement of the ancilla that controls the control-Z. b) The layout of Fig. 17 without considering depth.

circuit is of interest when analysing error-corrected circuits (it is influencing the number of physical qubits and the time to run the circuit), but not so much for NISQ circuits. However, there are trade offs when replacing Toffoli gates with ANDs and measurement-based uncomputations [36]. Moreover, in very hardware restricted environments it is the Clifford gate optimisation and not the T-gate optimisation that can save on resources.

Toffoli parallelisation is related to reducing the number of Hadamard gates: a Toffoli gate (also called CCX) is obtained from a double-controlled-Z gate (called CCZ) and two Hadamard gates. In a circuit consisting entirely of CCZ gates, all gates are trivially parallel and their Clifford+T implementation has constant depth when using the circuit from Fig. 8. However, adding Hadamard gates breaks the parallelism. Hadamard gates do not commute with the CCZ. Using the symbols existing in a circuit of Toffoli gates, it is not possible to trivially commute a control of a Toffoli gate with the target of another Toffoli gate: $\oplus \bullet \neq \bullet \oplus$. In other words, it is not possible to parallelise the Clifford+T decomposition of two Toffoli gates sharing a single qubit that is the target of the first Toffoli gate and the control of the second gate.

E. More Scheduling and Swapping in 3D

We present two other schedules for the Ctrl-Add and the third step of the multiplication circuit. Figs. 19 and 20 are the visualisation of the corresponding schedules of a single controlled-addition iteration, and Fig. 21 demonstrates the SWAP moments necessary after each iteration of controlled-addition.

```

1 Toffoli(ctrl, a3, z)
2 Toffoli(bj, a0, a1)
3 Toffoli(bj+1, a1, a2)
4 Toffoli(bj+2, a2, a3)
5 SWAP(bj+3, ctrl)
6 Toffoli(bj+3, a3, z)
7 SWAP(bj+3, ctrl), SWAP(a3, N)

```

```

8 SWAP(a3, z)
9 SWAP(z, E), SWAP(a3, bj+4)
10 Toffoli(ctrl, z, bj+4)
11 SWAP(bj+3, ctrl), SWAP(a3, bj+4), SWAP(z, N)
12 SWAP(z, a3)
13 SWAP(a3, E)
14 Toffoli(bj+3, a3, z)
15 SWAP(z, lower W)
16 SWAP(bj+3, z)
17 SWAP(z, ctrl), SWAP(bj+3, lower N)
18 for(k = n-1, k >=0; k--)
19   Toffoli(ctrl, ak, bj+k)
20   Toffoli(bj+k-1, ak-1, ak)
21   SWAP(ctrl, next clockwise ancilla), SWAP(
22     bj+k-1, next clockwise ancilla)
23   SWAP(ctrl, ak)
24   SWAP(ctrl, bj+k-1), SWAP(ak, next counter-
25   clockwise ancilla)
25   SWAP(ctrl, next counter-clockwise ancilla)
25 Toffoli(ctrl, a0, bj)

```

Listing 2. The j th iteration of the Ctrl-Add subcircuit, which repeats $N-1$ times in the multiplier circuit, running a setup subcircuit between each repetition after the first. Note that $ctrl = B_j$.

```

1. 1. SWAP(ctrl, queue above)
2. 2. SWAP(blowest, queue above)
3. for each cube k (besides the first):
4.   //this is all done in the same moment
5.   SWAP(ak, next counter-clockwise ancilla)
6.   SWAP(bj+k, ancillaabove)
7. 2. for each cube k (besides the first):
8.   //this is all done in the same moment
9.   SWAP(ak, next counter-clockwise ancilla)
10.  SWAP(bj+k, ancillaabove)
11.   SWAP(z, ancilla in the control position)
12.   SWAP(bj+n, N) //the ancilla above the next b
13.   in the queue
13. 3. SWAP(bj+n, W)
14. 4. SWAP(bj+n, z)
15. 5. SWAP(z, N), SWAP(bj+n, B-j+1)

```

Listing 3. The SWAP schedule immediately following the j -th iteration of the Ctrl-Add subcircuit.

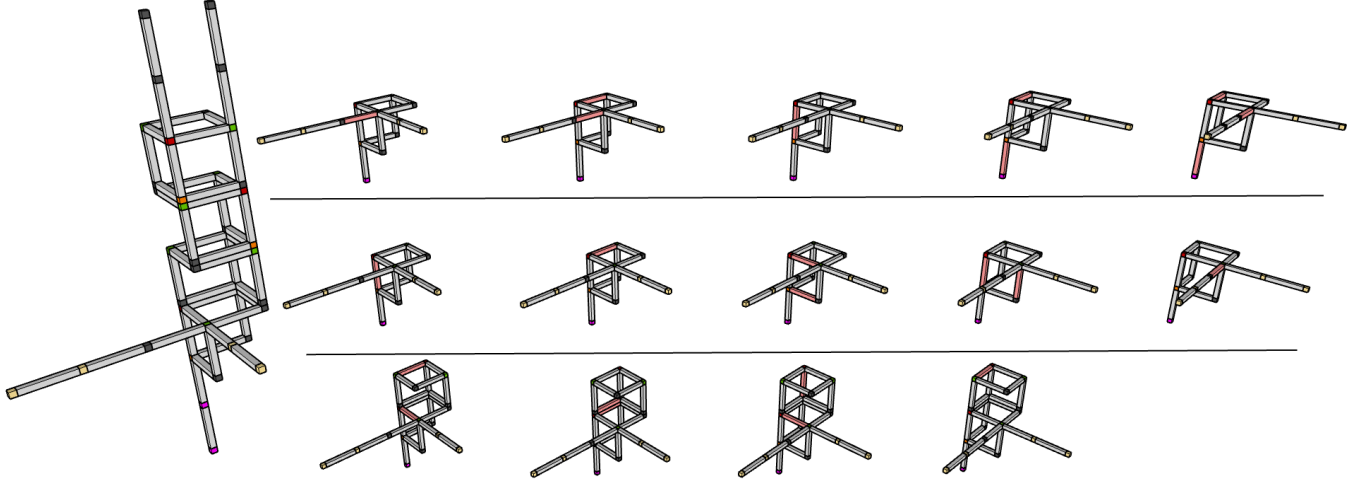


FIG. 19. Controlled-addition Step - SWAP schedule for the first part of the controlled-addition step of the 3D multiplier circuit, where a red bar indicates the application of a SWAP gate between two qubits. Time flows from left to right one row at a time. The logical operations to be performed on the circuit are applied between SWAP gates, as described in the schedule. By the end of one iteration of this step, one additional product qubit has been computed. Following the reset step, this step will be repeated for another iteration, and so on for $N-1$ iterations.

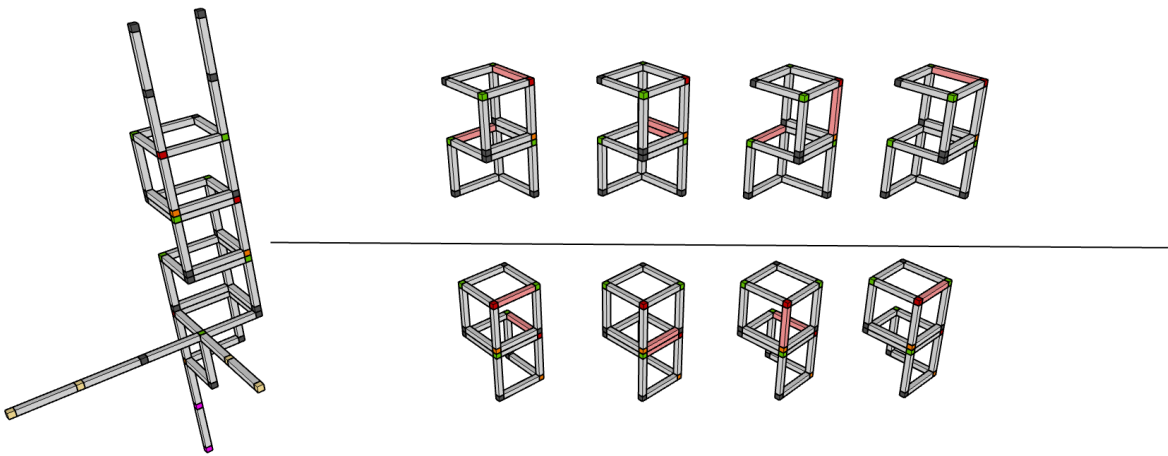


FIG. 20. Controlled-addition Step - SWAP schedule for the second part of the controlled-addition step of the 3D multiplier circuit, where a red bar indicates the application of a SWAP gate between two qubits. Time flows from left to right, one row at a time.

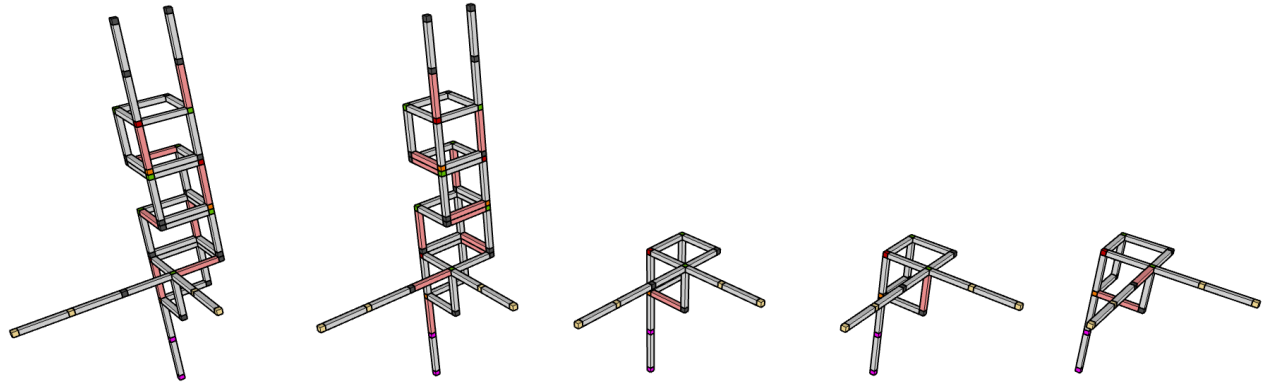


FIG. 21. Reset Step - SWAP schedule for the reset step of the 3D multiplier circuit, where a red bar indicates the application of a SWAP gate between two qubits. This step is applied following each iteration of the controlled-addition step. During this step, the control qubit (B_1 in the first iteration) is replaced by the next qubit in the B register. Time flows from left to right, one row at a time. Regardless of the size of the multiplication, this step always has a SWAP depth of 5.